

Activation Behavior of Boron and Phosphorus Atoms Implanted in Polycrystalline Silicon Films by Heat Treatment at 250°C

Toshiyuki SAMESHIMA, Nobuyuki ANDOH and Yasunori ANDOH¹

Tokyo University of Agriculture and Technology, 2-24-16 Naka-cho, Koganei, Tokyo 184-8588, Japan

¹*Nissin Ion Equipment. Co., Ltd., Kyoto 601-8205, Japan*

(Received May 21, 2004; accepted November 24, 2004; published March 8, 2005)

The activation behavior of boron and phosphorus implanted into laser-crystallized silicon films were investigated. The ratio of recrystallization of an ion-doping-induced amorphous region by heat treatment at 250°C was 0.35 for a boron concentration lower than $6.4 \times 10^{19} \text{ cm}^{-3}$ and 0.5 for a phosphorus concentration lower than $2.5 \times 10^{19} \text{ cm}^{-3}$. This ratio decreased as dopant concentration increased. High electrical conductivities of $1.1 \times 10^2 \text{ S/cm}$ and 7.3 S/cm were achieved by oxygen plasma treatment at 250°C for 1 h in the cases of $3.2 \times 10^{20} \text{ cm}^{-3}$ boron and $5.0 \times 10^{19} \text{ cm}^{-3}$ -phosphorus doping, respectively. Numerical analysis of the electrical conductivity revealed that the electrical conductivity was governed by recrystallization ratio and the density of the intrinsic defects of polycrystalline films. [DOI: 10.1143/JJAP.44.1186]

KEYWORDS: low-temperature activation, laser polycrystalline silicon, recrystallization, ion doping

1. Introduction

Low-temperature process technologies allow us to use inexpensive substrates such as glass substrates for fabricating thin film transistors (TFTs).^{1–4} Source and drain formation is one of the essential issues for TFT fabrication. Some technologies have been developed for low-temperature fabrication of TFTs.^{5–7} Ion doping is an attractive method for dopant incorporation into silicon films over a large area due to non-mass selection.⁸ In general, silicon films implanted with dopant atoms are annealed at a temperature above 400°C in order to activate the dopant atoms.⁹ Activation at a low temperature is necessary for establishing low-temperature fabrication processing of TFTs on cheap substrates such as glasses or plastics. A processing temperature below 300°C is required.

In this paper, we report the behaviors of dopant activation and carrier generation when polycrystalline silicon films implanted with boron and phosphorus atoms are heated at a low temperature of 250°C in air and oxygen plasma. We show that high recrystallization and activation ratios are achieved by low-temperature heat treatment under low-dopant-concentration conditions. We discuss the carrier generation properties in the doped silicon films.

2. Experimental

50-nm-thick amorphous silicon films were deposited by low pressure chemical vapor deposition (LPCVD). The silicon films were crystallized at room temperature in vacuum by irradiation with a pulsed XeCl excimer laser with a pulse width of 30 ns and a wavelength of 308 nm at an energy density of 360 mJ/cm^2 . Boron and phosphorus atoms were implanted into laser-crystallized silicon films by the ion doping method at 10 keV at room temperature. B_2H_6 gas and PH_3 gas were used as doping gas. The dopant concentrations ranged from 1.6×10^{13} to $1.6 \times 10^{15} \text{ cm}^{-2}$ for boron doping and from 1.0×10^{13} to $3.0 \times 10^{14} \text{ cm}^{-2}$ for phosphorus doping. Boron and phosphorus atoms were also implanted into single-crystal silicon and 50-nm-thick amorphous silicon films for comparison with poly-Si films. The analysis of secondary ion mass spectroscopy (SIMS) determined that boron atoms were entirely distributed in the silicon films. On the other hand, SIMS showed that

phosphorus atoms were concentrated 20 nm from the surface. Therefore the average volume concentrations ranged from 3.2×10^{18} to $3.2 \times 10^{20} \text{ cm}^{-3}$ for boron doping and from 5.0×10^{18} to $1.5 \times 10^{20} \text{ cm}^{-3}$ for phosphorus doping. Samples were then treated at 250°C with 100 W oxygen plasma at a pressure of 1.3 Torr and a gas flow rate of 100 sccm for 1 h.¹⁰ In this treatment, the samples were heated at 230–250°C for approximately 2 h including preheating and durations owing to the heating system. Some samples were heated in air at 250°C for 3 h for comparison. After the heat treatment, the crystalline volume ratio in the region 10 nm deep from the surface was estimated from the analysis of the optical reflectivity spectra in the ultraviolet region.^{11,12} For the estimation of the crystalline volume ratio, we used the peak around 276 nm (E_2 peak), which was caused by the large joint density of states at the X point in the Brillouin zone of crystalline silicon, while there was no peak for amorphous silicon. We calculated the optical reflectivity spectra of polycrystalline silicon films using a program including surface roughness and optical interference effects. The optical reflectivity spectra of polycrystalline silicon films ($R_{\text{calculated-poly-Si}}$) were obtained by combining the spectra of crystalline silicon films ($R_{\text{calculated-c-Si}}$) and with spectra of amorphous silicon films ($R_{\text{calculated-a-Si}}$) as

$$R_{\text{calculated-poly-Si}}(X) = X \times R_{\text{calculated-c-Si}} + (1 - X) \times R_{\text{calculated-a-Si}}, \quad (1)$$

where X is the crystalline volume ratio. The optimum crystalline volume ratio was determined by best fitting of optical reflectivity spectra to the experimental ones using the least-squares method for the difference between the calculated reflectivity, $R_{\text{calculated-poly-Si}}(X)$ and the experimental reflectivity, $R_{\text{experimental-poly-Si}}$. S was obtained by the summation of the square of difference between the calculated and experimental reflectivities for every wavelength using the following equation.

$$S(X) = \sum_{\lambda} [R_{\text{experimental-poly-Si}} - R_{\text{calculated-poly-Si}}(X)]^2 \quad (2)$$

The minimum S gave the most possible crystalline volume ratio, X . The minimum S had still an uncertainty because of the accuracy of reflectivity measurements ΔR . At the minimum S as a function of X ,

$$\begin{aligned} \Delta S &= \sum_{\lambda} \left| \frac{\partial S}{\partial R_{\text{experimental}}} \right| \Delta R_{\text{experimental}} + \left| \frac{\partial S}{\partial X} \right| \Delta X \\ &= \sum_{\lambda} \left| \frac{\partial S}{\partial R_{\text{experimental}}} \right| \Delta R_{\text{experimental}}. \end{aligned}$$

We assumed that the accuracy of the crystalline volume ratio, (ΔX), is governed by

$$\begin{aligned} \left| \frac{\partial S}{\partial X} \right| \Delta X &\equiv \sum_{\lambda} \left| \frac{\partial S}{\partial R_{\text{calculated}}} \right| \left| \frac{\partial R_{\text{calculated}}}{\partial X} \right| \Delta X \\ &= \sum_{\lambda} \left| \frac{\partial S}{\partial R_{\text{experimental}}} \right| \Delta R_{\text{experimental}}. \end{aligned} \quad (3)$$

Thus

$$\begin{aligned} \Delta X &= \left[\sum_{\lambda} \left| \frac{\partial S}{\partial R_{\text{calculated}}} \right| \left| \frac{\partial R_{\text{calculated}}}{\partial X} \right| \right]^{-1} \\ &\quad \times \left[\sum_{\lambda} \left| \frac{\partial S}{\partial R_{\text{experimental}}} \right| \right] \Delta R_{\text{experimental}} \\ &\approx \left[\sum_{\lambda} \left| \frac{\partial S}{\partial R_{\text{calculated}}} \right| \left| \frac{\partial R_{\text{calculated}}}{\partial X} \right| \right]^{-1} \\ &\quad \times \left[\sum_{\lambda} \left| \frac{\partial S}{\partial R_{\text{calculated}}} \right| \right] \Delta R_{\text{experimental}} \end{aligned} \quad (4)$$

because the calculated reflectivity was close to the experimental reflectivity in the best fitting.

$$\left[\sum_{\lambda} \left| \frac{\partial S}{\partial R_{\text{calculated}}} \right| \left| \frac{\partial R_{\text{calculated}}}{\partial X} \right| \right]^{-1} \left[\sum_{\lambda} \left| \frac{\partial S}{\partial R_{\text{calculated}}} \right| \right]$$

ranged from 0.2 to 3 for X from 0.9 to 0.1 and ΔR was 0.01 in this experiment. ΔX was therefore 0.03 at most. Visible range spectra were also analyzed in order to estimate the thicknesses of the top amorphous region underlying crystalline region when no E_2 peak was observed due to complete amorphous states at the surface region. The electrical conductivity was also measured with Al gap electrodes formed by thermal evaporation.

3. Results and Discussion

Figure 1 shows the optical reflectivity spectra of single-crystal silicon (a) and 50-nm-thick amorphous silicon films (b). The figure includes the spectra of initial materials, as implanted of phosphorus ion of $3.0 \times 10^{19} \text{ cm}^{-3}$ and as annealed for 3 h at 250°C in air. The height of E_2 peak, which appeared around a wavelength of 276 nm, was reduced by phosphorus implantation as shown in Fig. 1(a). The decrease in E_2 peak height indicates the formation of disordered amorphous states caused by phosphorus doping. The E_2 peak height was increased by annealing in air at 250°C for 3 h. This means that the heat treatment caused recrystallization of the disordered amorphous states. On the other hand, there was no E_2 peak in the spectra of the initial amorphous silicon films as shown in Fig. 1(b). Moreover, no E_2 peak appeared through phosphorus implantation followed by the heat treatment at 250°C . The disordered amorphous region caused by phosphorus implantation was not crystallized by the heat treatment in the case of amorphous silicon

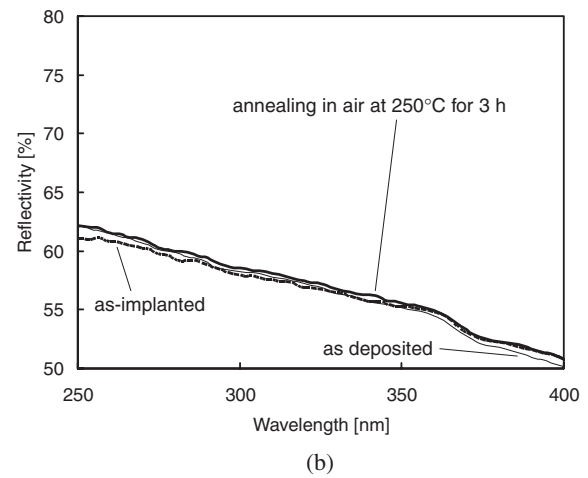
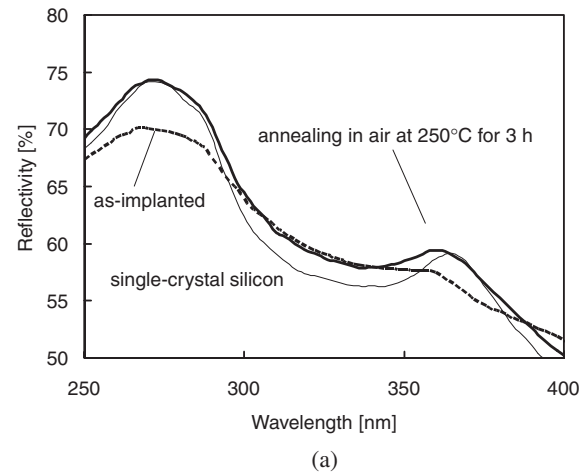


Fig. 1. Optical reflectivity spectra for $3.0 \times 10^{19} \text{ cm}^{-3}$ phosphorus implanted single-crystal silicon (a) and 50-nm-thick amorphous silicon films (b) before and after annealing treatment for 3 h at 250°C .

films. These results shown in Fig. 1 suggest that the recrystallization of the disordered region formed by ion implantation at low temperature of 250°C needs the crystalline nucleation site. Crystalline silicon still had a high E_2 peak just after phosphorus implantation as shown in Fig. 1(a). This means that crystalline regions remained in the surface region. They probably played a role in crystalline nucleation and induced the recrystallization of the disordered amorphous silicon region. On the other hand, there was no chance of recrystallization of the disordered region formed by ion implantation because of no crystalline nucleation for amorphous silicon. We believe that crystalline nucleation is essential for the recrystallization of the disordered amorphous region by heat treatment at the low temperature of 250°C .

Figure 2 shows the optical reflectivity spectra for 50-nm-thick silicon films implanted with different boron concentrations. The as-crystallized silicon films at 360 mJ/cm^2 had a large E_2 peak around 276 nm. The crystalline volume ratio was 0.84 for as-crystallized silicon films. The E_2 peak height was reduced as the boron concentration increased, as shown in Fig. 1. This means that amorphous regions were formed by boron doping.

Figure 3(a) shows the crystalline volume ratio as functions of boron concentration. It decreased from 0.78 to 0.09

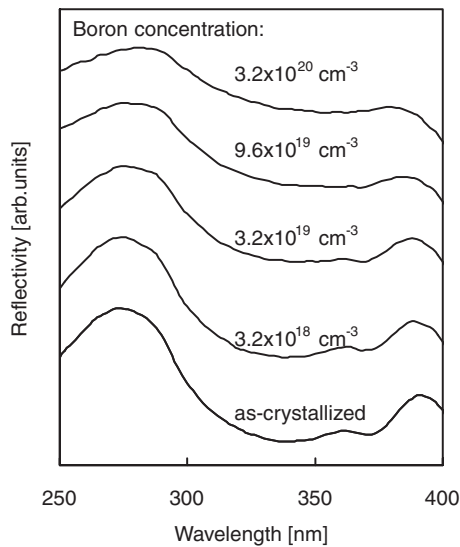


Fig. 2. Optical reflectivity spectra for 50-nm-thick silicon films crystallized using 360 mJ/cm^2 excimer-laser irradiation, which were implanted with different boron concentrations at 10 keV.

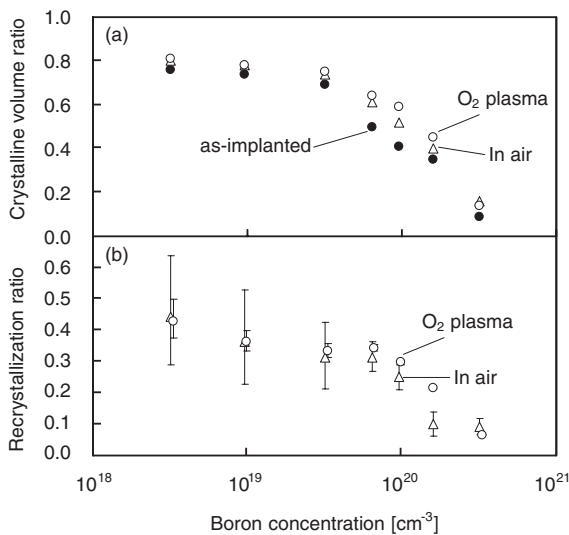


Fig. 3. Crystalline volume ratio (a) and recrystallization ratio (b) of amorphous states as functions of boron concentration for 250°C heat treatments in air for 3 h and in 100 W oxygen plasma for 1 h.

as the boron concentration increased from 3.2×10^{18} to $3.2 \times 10^{20} \text{ cm}^{-3}$. The reduction of the crystalline volume ratio with boron doping indicates that boron ion bombardment destroyed the crystalline state. A significant increase in the crystalline volume ratio was observed by the 250°C heat treatments in air as well as in oxygen plasma, as shown in Fig. 3(a). The disordered amorphous regions formed by boron doping were partially crystallized again by the heat treatments at 250°C . Figure 3(b) shows the recrystallization ratio of amorphous states by heat treatment as $\{X(\text{annealed}) - X(\text{implanted})\} / \{X(\text{initial}) - X(\text{implanted})\}$. For the doping concentration below $6.4 \times 10^{19} \text{ cm}^{-3}$, 35% of the amorphous regions were changed to crystalline states by the heat treatment. The effective recrystallization probably occurred by the fact that the residual crystalline regions surrounding amorphous regions played a role of

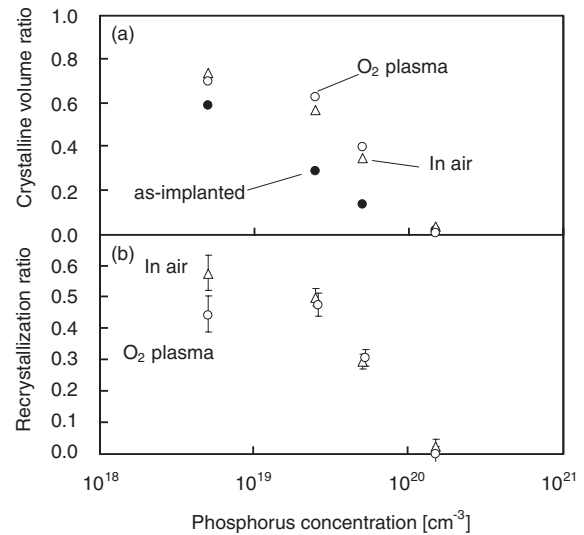


Fig. 4. Crystalline volume ratio (a) and recrystallization ratio (b) of amorphous states as functions of phosphorus concentration for 250°C heat treatments in air and in oxygen plasma.

nucleation sites for recrystallization. When the boron concentration was low, amorphous regions formed by boron doping were isolated from each other. There were many crystalline nucleation sites around the amorphous region. This would cause effective recrystallization by heat treatment. On the other hand, the recrystallization ratio was reduced to approximately 0.09 as the doping concentration increased to $3.2 \times 10^{20} \text{ cm}^{-3}$, as shown in Fig. 3(b). The doping with a high boron concentration causes high-density amorphous regions to overlap each other. The increase of the amorphous regions and their overlapping reduced the density of crystalline nucleation sites. Therefore, recrystallization ratio decreased as boron concentration increased. Heat treatment in air and in oxygen plasma resulted in similar crystalline volume ratios and recrystallization ratios for each boron concentration. This means that recrystallization was simply governed by temperature for heat treatment.

Figure 4 shows crystalline volume ratio (a) and recrystallization ratio by heat treatment (b) as functions of phosphorus concentration. The crystalline volume ratio decreased from 0.6 to 0.01 (resolution limit) as the phosphorus concentration increased from 5.0×10^{18} to $1.5 \times 10^{20} \text{ cm}^{-3}$. The phosphorus ion bombardment changed the crystalline state to amorphous more markedly than boron doping because of the high impulse due to heavy mass. A significant increase in crystalline volume ratio was observed by the 250°C heat treatments in air and in oxygen plasma as shown in Fig. 4(b). For a doping concentration below $2.5 \times 10^{19} \text{ cm}^{-3}$, 50% of the amorphous regions were changed to crystalline states. The recrystallization ratio was reduced to 0.01 as the doping concentration increased to $1.5 \times 10^{20} \text{ cm}^{-3}$. The amorphous region markedly increased at the surface region. The recrystallization region markedly decreased with increasing phosphorus concentration compared with that of the boron doping case. For $1.5 \times 10^{20} \text{ cm}^{-3}$ -phosphorus doping, the E_2 peak analysis revealed that the surface region was still in an almost amorphous state after the heat treatment. However, there were residual crystallization regions at the bottom region of

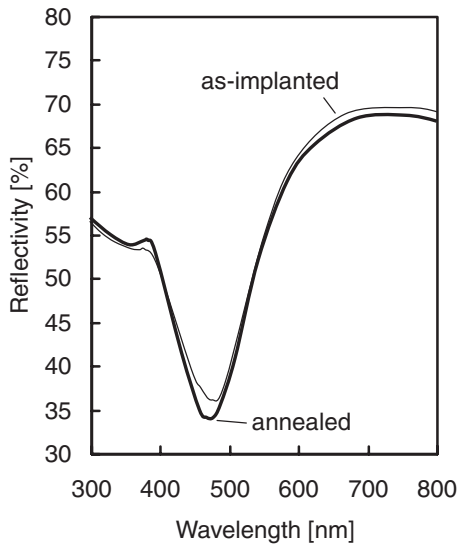


Fig. 5. Optical reflectivity spectra in visible wavelength region for phosphorus-doped silicon with $1.5 \times 10^{20} \text{ cm}^{-3}$ for as-implanted case and 250°C heat treatment in air for 3 h.

the film near the glass interface for phosphorus doping because the amorphous regions were limited to the surface region. The underlying crystallized regions probably acted as crystalline nucleation sites. The optical spectra in visible wavelength were changed by the 250°C heat treatment, as shown in Fig. 5. The optical reflectivity decreased at approximately 480 nm because of the optical interference effect. The reflectivity at the valley further decreased after the heat treatment. This means that the optical interference was more effective because the degree of the optical absorption was reduced after the heat treatment. The analysis of the optical spectra revealed that as-implanted samples consisted of a 20-nm-thick top amorphous region and 30-nm-thick bottom crystalline silicon region with a crystalline volume ratio of 0.84. The heat treatment reduced the thickness of the amorphous layer to 18 nm and increased that of the crystalline layer to 32 nm. This means that the recrystallization of the overlying amorphous region proceeded from underlying crystalline region. The recrystallization ratio for heat treatment in air and oxygen plasma shows similar characteristics as a function of phosphorus concentration. Recrystallization was governed by temperature for heat treatment similar to that in the boron doping case.

Figure 6 shows the electrical conductivity as a function of boron volume concentration. The electrical conductivity of amorphous silicon implanted at a boron concentration of $3.2 \times 10^{19} \text{ cm}^{-3}$ is also shown. The electrical conductivities of boron-doped amorphous silicon as-implanted and as-annealed in air for 3 h were very low, ranging from 10^{-4} to 10^{-6} S/cm . This means that the carrier density in the amorphous region was negligible. The electrical conductivity increased from 2.8×10^{-5} to 8.0 S/cm as the boron concentration increased from 3.2×10^{18} to $3.2 \times 10^{20} \text{ cm}^{-3}$ for the as-implanted case. This indicates that some boron atoms were activated and free carriers were generated. The electrical conductivity was markedly increased from 4.0×10^{-3} to $1.1 \times 10^2 \text{ S/cm}$ by heat treatment in air at 250°C as the boron concentration increased. It was also increased

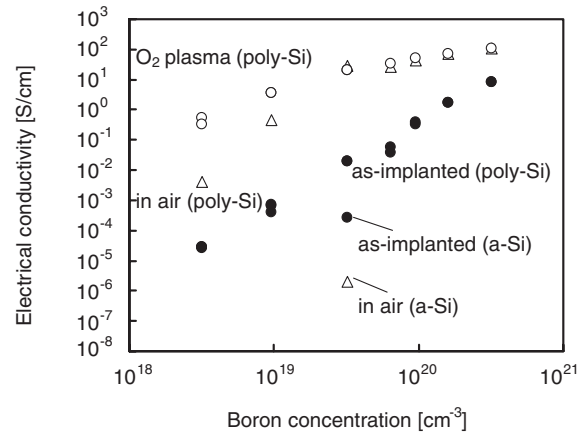


Fig. 6. Electrical conductivity as a function of boron concentration for as-implanted, 250°C heat treatments in air and in oxygen plasma. The data in the case of ion doping to amorphous silicon is also shown.

from 5.5×10^{-1} to $1.1 \times 10^2 \text{ S/cm}$ by oxygen plasma treatment at 250°C as the boron concentration increased. Both heat treatments increased the electrical conductivities to almost the same values for boron concentration above $3.2 \times 10^{19} \text{ cm}^{-3}$. On the other hand, the samples heated with oxygen plasma had a higher electrical conductivity than the samples heated in air for a boron concentration below $3.2 \times 10^{19} \text{ cm}^{-3}$. This indicates that defect states trapping carriers seriously affected the electrical conductivity for a boron concentration below $3.2 \times 10^{19} \text{ cm}^{-3}$. Electrical conductivity was measured and analyzed with a numerical calculation program. Dopant atoms were assumed to be uniformly distributed in amorphous regions formed by doping, and to be activated according to recrystallization by heat treatment. Activated boron concentration was therefore described as $N_{\text{dopant}} \times R$, where N_{dopant} denotes the doping concentration and R the recrystallization ratio. There are two possible reasons for defect states trapping carriers. One is that intrinsic defect states existed in polycrystalline films formed by laser crystallization. The density of intrinsic defect states, N_i , with deep energy levels was on the order of 10^{18} cm^{-3} for as-crystallized samples.¹³⁾ We have revealed that oxygen plasma at 250°C effectively reduces the density of intrinsic defects to a level on the order of 10^{17} cm^{-3} by the oxidation of the electrical active defects associated with dangling bonds. After oxygen plasma treatment, the density of defects is given by $A \times N_i$, where A is the defect reduction factor by oxygen plasma. The other is defect states formed by ion doping. The defect density induced by ion doping would be proportional to the doping concentration. We also assumed that the density of defect states caused by doping was reduced according to recrystallization by heat treatment and also changed to electrical inactive by oxygen plasma treatment like intrinsic defects. The defect density is therefore $(1 - R) \times A \times B \times N_{\text{dopant}}$ for the oxygen plasma case, where B is a proportional factor giving the density defect states formed by ion doping. The hole concentration, h , was given using charge neutrality conditions as,

$$h = (1 - f(E_f, E_d, T))N_d R - f(E_f, E_t, T) \times (A \times N_i + (1 - R)A \times B \times N_{\text{dopant}}),$$

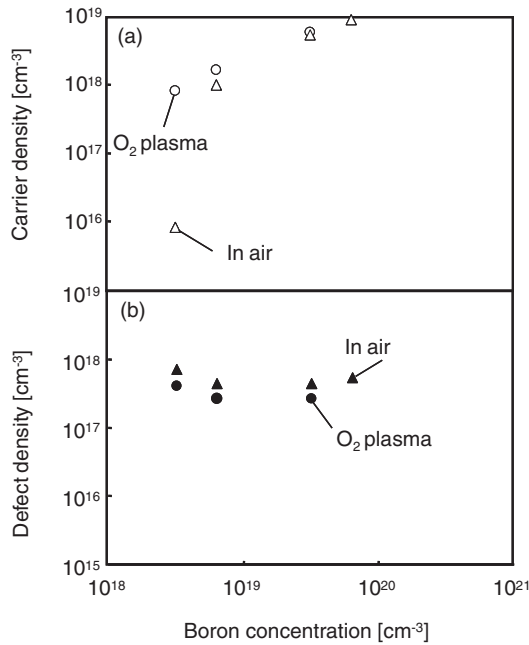


Fig. 7. Average carrier density (a) after heat treatments and density of total defect states (b) as functions of boron doping concentration.

where f is the Fermi–Dirac distribution function with the Fermi level E_f , the dopant energy level E_d , the temperature T , and the energy level of defects E_t . We assumed that the defect states were located at the midgap so that their energy level E_t was 0.55 eV. Using the conditions described above, we carefully analyzed the electrical conductivity with different temperatures around room temperature between 20°C and 60°C for each doping concentration and determined the parameters of A and B . The analysis gave the average carrier density after heat treatment and the total defect states as functions of boron doping concentration, as shown in Fig. 7. The carrier densities were $5.3 \times 10^{18} \text{ cm}^{-3}$ and $8.9 \times 10^{18} \text{ cm}^{-3}$ for the boron concentrations of 3.2×10^{19} and $6.4 \times 10^{20} \text{ cm}^{-3}$, respectively, for heat treatment in air and oxygen plasma, as shown in Fig. 7(a). On the other hand, the carrier density for oxygen plasma treatment was higher than that for heat treatment in air. The numerical analysis revealed that the total defect density was $7 \times 10^{17} \text{ cm}^{-3}$ for heat treatment in air and $3 \times 10^{17} \text{ cm}^{-3}$ for heat treatment in oxygen plasma. Defect density was almost independent of boron concentration. This means that the carrier trapping was governed by the intrinsic defects formed by laser crystallization. The defect caused by impurity doping was not serious under the present conditions. The decrease in the density of the defect states by oxygen plasma treatment increased the carrier density for low doping concentrations.

Figure 8 shows electrical conductivity as a function of phosphorus concentration. The electrical conductivities of $3.0 \times 10^{19} \text{ cm}^{-3}$ implanted amorphous silicon before and after annealing are also shown. Both the above electrical conductivities were low and ranged from 10^{-7} to 10^{-8} S/cm . The electrical conductivity was very low ranging from 10^{-5} to 10^{-4} S/cm for concentrations between 5.0×10^{18} and $1.5 \times 10^{20} \text{ cm}^{-3}$ for the as-implanted case. No activation was observed for the as-implanted case. Electrical conduc-

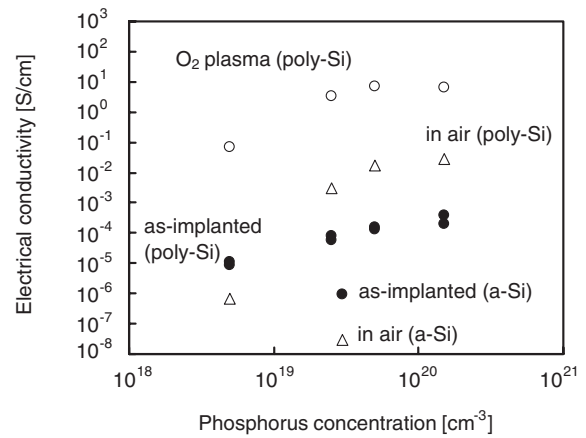


Fig. 8. Electrical conductivity as a function of phosphorus concentration for as-implanted case, 250°C heat treatments in air and in oxygen plasma.

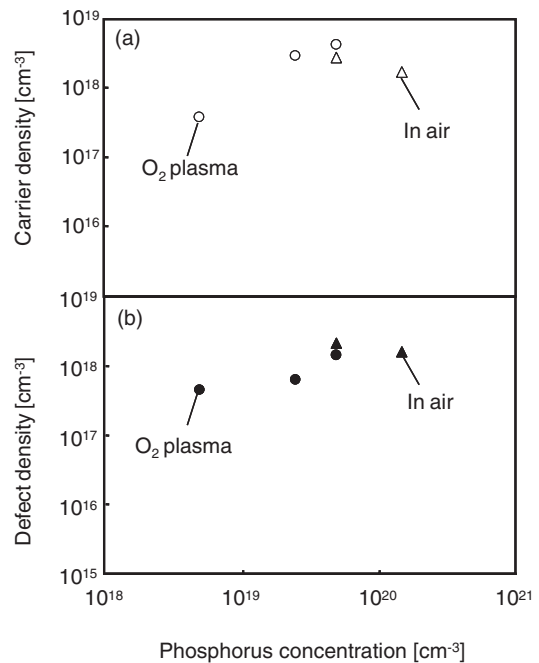


Fig. 9. Average carrier density (a) after heat treatments and density of total defect states (b) as functions of phosphorus doping concentration.

tivity increased from 1.0×10^{-6} to $2.8 \times 10^{-2} \text{ S/cm}$ by heat treatment in air at 250°C as phosphorus concentration increased. On the other hand, oxygen plasma treatment at 250°C markedly increased from 7.0×10^{-2} to 7.1 S/cm as phosphorus concentration increased to $5.0 \times 10^{19} \text{ cm}^{-3}$. The significantly different electrical conductivities between heat treatment in air and oxygen plasma indicate that a decrease in the density of the defects in the oxygen plasma is essential for carrier generation in the case of phosphorus doping. The electrical conductivity was analyzed using the model described above. Figure 9 shows the average carrier density (a) after heat treatment and the density of total defect states (b) as functions of phosphorus doping concentration. The carrier densities were $2.8 \times 10^{18} \text{ cm}^{-3}$ and $4.0 \times 10^{18} \text{ cm}^{-3}$ for the phosphorus concentrations of 2.5×10^{19} and $5.0 \times 10^{19} \text{ cm}^{-3}$, respectively, for heat treatment in oxygen plasma, as shown in Fig. 9(a). On the other hand, a low

carrier density of $3.0 \times 10^{17} \text{ cm}^{-3}$ was observed for $5.0 \times 10^{18} \text{ cm}^{-3}$ doping because of electron carrier trapping at the density of defect states. The density of defect states trapping electrons ranged from 5×10^{17} to $1.4 \times 10^{18} \text{ cm}^{-3}$ for the oxygen plasma case. It was higher than that of trapping holes, as shown in Figs. 7(b) and 9(b). It slightly increased to $1 \times 10^{18} \text{ cm}^{-3}$ as the phosphorus doping concentration increased to $5.0 \times 10^{19} \text{ cm}^{-3}$. Although the electron carrier trapping was governed by the intrinsic defects formed by laser crystallization, there is a possibility of defects being formed by impurity doping, whose degree was approximately 0.02/phosphorus-atom after oxygen plasma treatment.

4. Summary

The activation behaviors of boron and phosphorus implanted into laser-crystallized silicon films were investigated. 50-nm-thick silicon films were crystallized by XeCl excimer laser irradiation. They were doped with boron and phosphorus by 10-keV-ion doping. Ion doping induced amorphous states in the poly-Si films because of their ion bombardment. Heat treatments at 250°C for 3 h in air and for 1 h in 100 W oxygen plasma were carried out to recrystallize amorphous regions. The analysis of UV and visible optical reflectivity spectra revealed that recrystallization occurred via heat treatment at 250°C under the existence of the crystalline nucleation site. High recrystallization ratios were achieved: 0.35 for boron concentrations lower than $6.4 \times 10^{19} \text{ cm}^{-3}$ and 0.5 for phosphorus concentrations lower than $2.5 \times 10^{19} \text{ cm}^{-3}$. The recrystallization ratios at the surface region were reduced to 0.09 as boron concentration increased to $3.2 \times 10^{20} \text{ cm}^{-3}$ and to 0.01 as phosphorus concentration increased to $1.5 \times 10^{20} \text{ cm}^{-3}$. An extremely amor-

phous region remained in the cases of high doping concentration. Electrical conductivities of $1.1 \times 10^2 \text{ S/cm}$ and 7.3 S/cm were achieved for $3.2 \times 10^{20} \text{ cm}^{-3}$ boron and $5.0 \times 10^{19} \text{ cm}^{-3}$ phosphorus dopings, respectively, because recrystallization induced by 250°C heat treatments caused the activation of boron and phosphorus atoms. Numerical analysis of the electrical conductivity revealed that the electrical conductivity was governed by activation ratio and the density of the intrinsic defects of poly-Si films. Oxygen plasma treatment resulted in high electrical conductivity due to the increase in effective carrier density caused by the decrease in the density of electrically active defects.

- 1) T. Sameshima, S. Usui and M. Sekiya: *IEEE Electron Device Lett.* **7** (1986) 276.
- 2) K. Sera, F. Okumura, H. Uchida, S. Itoh, S. Kaneko and K. Hotta: *IEEE Trans. Electron Devices* **36** (1989) 2868.
- 3) T. Serikawa, S. Shirai, A. Okamoto and S. Suyama: *Jpn. J. Appl. Phys.* **28** (1989) L1871.
- 4) A. Kohno, T. Sameshima, N. Sano, M. Sekiya and M. Hara: *IEEE Trans. Electron Devices* **42** (1995) 251.
- 5) T. Sameshima, K. Saitoh, N. Aoyama, S. Higashi, M. Kondo and A. Matsuda: *Jpn. J. Appl. Phys.* **38** (1999) 1892.
- 6) Y. Tsunoda, T. Sameshima and S. Higashi: *Jpn. J. Appl. Phys.* **39** (2000) 1656.
- 7) T. Watanabe, N. Andoh and T. Sameshima: *Mater. Res. Soc. Symp. Proc.* **664** (2001) A.6.10.1-6.
- 8) A. Yoshida, M. Nukayama, Y. Andoh, M. Kitagawa and T. Hirao: *Jpn. J. Appl. Phys.* **30** (1991) L67.
- 9) Y. Mishima and M. Takei: *J. Appl. Phys.* **75** (1994) 4933.
- 10) H. Watakabe and T. Sameshima: *Appl. Phys. A* **77** (2003) 141.
- 11) T. Sameshima: *Mater. Res. Soc. Symp. Proc.* **536** (1999) 427.
- 12) T. Sameshima, K. Saitoh, N. Aoyama, S. Higashi, M. Kondo and A. Matsuda: *Jpn. J. Appl. Phys.* **38** (1999) 1892.
- 13) K. Asada, K. Sakamoto, T. Watanabe, T. Sameshima and S. Higashi: *Jpn. J. Appl. Phys.* **39** (2000) 3883.